Proceedings of the Seventh International Conference on
Railway Technology: Research, Development and Maintenance
Edited by: J. Pombo
Civil-Comp Conferences, Volume 15, Paper 11.16
Civil-Comp Press, Edinburgh, United Kingdom, 2026
ISSN: 2753-3239, doi: 10.4203/ccc.15.11.16

Capacity Configuration Optimization of High-Speed Maglev Traction Power Supply System Based on DAB and Energy Storage System

L. Zhang[1,2,3,4], Y. Zhao[1,2,3,4], G. Lin[1,2,3,4], H. Wang[1,2,3,4] and Y. Luo[1,2,3,5]

[1]College of Transportation, Tongji University, Shanghai, China
[2]National Maglev Transportation Engineering R&D Center, Tongji University, Shanghai, China
[3]Key Laboratory of Maglev Technology in Railway Industry, Tongji University, Shanghai, China
[4]State Key Laboratory of High-speed Maglev Transportation Technology, Tongji University, Shanghai, China
[5]School of Mechanical Engineering, Tongji University, Shanghai, China

Abstract

This paper proposes a high-speed maglev traction power supply system architecture integrating a supercapacitor energy storage system and dual active bridge converters to realize efficient regenerative braking energy recovery and cross-zone utilization. A bi-level optimization model is established, incorporating both operation scheduling and capacity configuration. The inner level formulates a rule-based energy management strategy that dynamically coordinates real-time power allocation among subsystems according to traction load operating characteristics. The outer level develops a multi-objective capacity configuration optimization model with the objectives of minimizing the total lifecycle cost and maximizing the regenerative braking energy utilization rate, and obtains the optimal capacity configuration scheme. Simulation results demonstrate that the proposed method achieves an optimal system configuration, increasing the regenerative braking energy utilization rate to 99.36%, reducing the maximum demand by 20.11%, and lowering the total system lifecycle cost by 9.72%.

Keywords: high-speed maglev, regenerative braking energy, dual active bridge converter, energy storage system, multi-objective optimization, capacity configuration.

1 Introduction

High-speed maglev transportation possesses significant characteristics such as high speed, low noise, high comfort, and strong climbing capability, making it a critical component for building a comprehensive, efficient, modern transportation network and supporting the national strategy of strengthening transportation infrastructure[1]. However, under the backdrop of the national "dual carbon" strategy and the transition towards energy-saving and low-carbon transportation systems, the energy consumption issue of high-speed maglev trains becomes increasingly prominent as they advance towards the 600 km/h speed level, facing immense pressure for energy conservation and emission reduction. Studies indicate that the braking energy can reach 20%–30% of the traction energy[2]. Nevertheless, constrained by characteristics such as the uncontrolled rectifier power supply architecture and independent segmented power supply zones, regenerative braking energy (RBE) cannot be directly fed back to the public grid or reused by other trains under traction conditions. This energy can only be dissipated directly onto braking resistors, resulting in a near-zero energy utilization rate and causing substantial energy waste[3].

In the field of conventional wheel-rail transportation, solutions for RBE recovery and utilization are relatively mature, primarily encompassing two technical routes: on-site energy storage consumption and energy feedback transfer. Although configuring ground-based energy storage systems (ESSs), such as supercapacitors or flywheels, can effectively absorb RBE and smooth load fluctuations[4], the power demand of high-speed maglev trains is extremely high, and relying solely on a local ESS to fully absorb the train's RBE incurs substantial initial investment costs. On the other hand, energy transfer schemes based on inverter feedback[5] or railway power conditioners (RPC)[6], while capable of energy inversion, feedback, and transfer, are difficult to apply directly to high-speed maglev transportation due to its special AC-DC-AC traction power supply system (TPSS). Considering the complementary operating conditions of trains in adjacent power supply zones of high-speed maglev lines, this paper introduces the dual active bridge (DAB) converter to break the electrical isolation of physical power supply zones and enable cross-zone energy mutual support between adjacent zones. However, a single cross-zone interconnection cannot address non-complementary conditions, such as simultaneous traction or braking of trains in adjacent zones. Therefore, establishing a traction power supply architecture that integrates an ESS and cross-zone interconnected DAB converters becomes key to solving the challenge of efficient RBE utilization in high-speed maglev systems.

The technical and economic benefits of the modified TPSS architecture heavily depend on the optimal capacity configuration of core equipment, and numerous scholars have conducted research on capacity configuration optimization methods for different architectures. Reference [7] proposed an integrated capacity configuration design method that coordinates long-term system planning and short-timescale real-time control for a hybrid energy storage-integrated railway power flow conditioner (RPFC) architecture in the electrified railway domain. Reference [8] proposed a bi-level model capacity configuration method that balances economic investment costs and comprehensive operational performance for a flexible smart TPSS architecture in the electrified railway domain. Reference [9] proposed a capacity configuration method that ensures DC bus voltage stability and ESS economic benefits for a hybrid ESS architecture in the DC microgrid domain. Reference [10] proposed a bi-level collaborative capacity optimization configuration method considering system sizing and control strategies for a hybrid ESS architecture in the urban rail transit domain. While the above studies provide some feasible research ideas for the capacity configuration optimization methods of modified traction power supply systems, research on the capacity configuration optimization method for the proposed high-speed maglev TPSS integrating an ESS and DAB cross-zone interconnection remains a gap that urgently needs to be explored.

To address the above issues, this paper first proposes a high-speed maglev traction power supply architecture integrating an ESS and cross-zone interconnected DAB converters based on the characteristics of the high-speed maglev TPSS. Subsequently, an energy management strategy that considers both system operational stability and economy is formulated by combining the operating characteristics of traction loads with the characteristics of the ESS and DAB. Then, with the minimization of the total system lifecycle cost and the maximization of the energy utilization rate as objective functions, the Nondominated Sorting Genetic Algorithm II (NSGA-II) is employed for global optimal solving, and the Technique for Order Preference by Similarity to Ideal Solution (TOPSIS) is introduced to compromise and obtain the optimal capacity configuration scheme. Finally, a comparative case study analysis validates the correctness and effectiveness of the proposed method.

2 Methods

2.1 System Architecture

As shown in Fig. 1, based on the original high-speed maglev TPSS, this paper deploys a set of supercapacitor ESS on the DC bus of each of two adjacent power supply zones, and connects the DC buses of adjacent zones via a DAB converter, thereby providing a spatial transfer path for RBE. For ease of description, the tracks corresponding to the two adjacent zones in the high-speed maglev TPSS are designated as Track i and Track j, respectively.

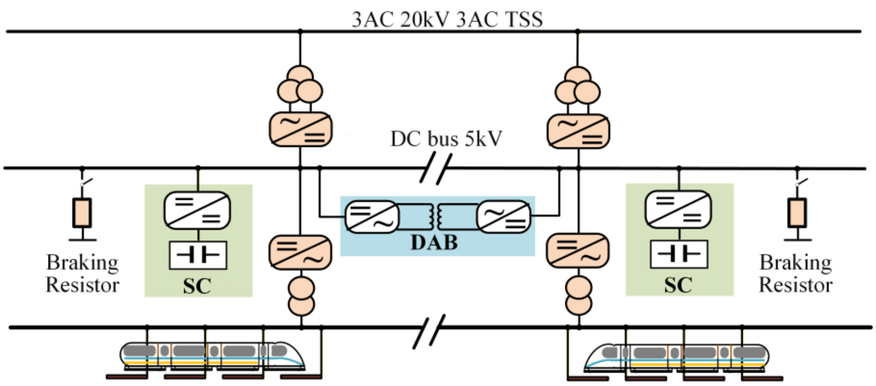

Figure 1: Architecture of the high-speed maglev TPSS integrating a supercapacitor ESS and DAB converters.

At any time instant t ,for Track $k \in \{i,j\}$, the power balance equation at the DC bus is expressed as:

$$P_{grid,k}(t) + P_{SC,k}(t) + P_{DAB,k}(t) = P_{load,k}(t) + P_{R,k}(t) \tag{1}$$

Where $P_{grid,k}(t)$ is the output power from the grid; $P_{SC,k}(t)$ is the power of the SESS, defined as positive for discharging and negative for charging; $P_{DAB,k}(t)$ is the power transferred through the DAB, defined as positive for power flowing in and negative for power flowing out; $P_{load,k}(t)$ is the traction load power, defined as positive during motoring and negative during braking ; $P_{R,k}(t)$ is the power consumed by the braking resistor, satisfying $P_{R,i}(t) \geq 0$.

2.2 Rule-Based Energy Management Strategy

To address the coordinated energy interaction problem among subsystems under various operating conditions and to maximize RBE utilization and peak shaving and valley filling of the traction load, this paper formulates a rule-based energy management strategy. The specific energy scheduling process is divided into the following two stages:

Stage 1: Cross-Section Energy Sharing

When the trains in adjacent power supply zones are in complementary operating conditions, i.e., one train is braking while the other is traction, the DAB converter is activated to transfer RBE from the braking track to the traction track for traction power supply. Taking the case where the train on Track i is braking ($P_{load,i} < 0$) and the train on Track j is traction ($P_{load,j} > 0$) as an example, the transmission powers of the DAB for Track i and Track j at this moment are:

$$\begin{cases} P_{DAB,j}(t) = \min\left(|P_{load,i}(t)|\eta_{DAB},\ P_{load,j}(t),\ P_{DAB}^{N}\right) \\ P_{DAB,i}(t) = -\dfrac{P_{DAB,j}(t)}{\eta_{DAB}} \end{cases} \tag{2}$$

where P_{DAB}^{N} is the rated power capacity of the DAB converter and η_{DAB} is its power transfer efficiency. When the adjacent sections are in other combinations of operating conditions, the DAB ceases operation, at which point:

$$P_{DAB,i}(t) = P_{DAB,j}(t) = 0 \tag{3}$$

Stage 2 Local Energy Storage Scheduling

After Stage 1, the residual load $P_{adj,k}(t)$ that must be handled locally by each power supply section is:

$$P_{adj,k}(t) = P_{load,k}(t) - P_{DAB,k}(t) \tag{4}$$

If $P_{adj,k}(t) > 0$, it indicates that Track k still has traction demand. The ESS is activated first to supply power for train traction, and any portion exceeding its supply capability is supplemented by the power grid. The power of each subsystem under this condition is:

$$\begin{cases} P_{SC,k}(t) = P_{adj,k}(t) \\ P_{grid,k}(t) = P_{adj,k}(t) - P_{SC,k}(t) \\ P_{R,k}(t) = 0 \end{cases} \tag{5}$$

where $P^N_{SC,k}$ is the rated power of the supercapacitor.

If $P_{adj,k}(t) < 0$, it indicates that Track k still has surplus RBE. The ESS is activated first to recover energy, and any RBE exceeding its recovery capability is dissipated by the braking resistor. The power of each subsystem under this condition is:

$$\begin{cases} P_{SC,k}(t) = P_{adj,k}(t) \\ P_{R,k}(t) = |P_{adj,k}(t)| - |P_{SC,k}(t)| \\ P_{grid,k}(t) = 0 \end{cases} \tag{6}$$

2.3 Multi-Objective Optimization Model

The multi-objective optimization model aims to optimize the rated configuration of key equipment while balancing economic and technical performance. Considering the spatiotemporal distribution differences of traction loads, the ESSs in adjacent power supply zones are configured separately. Therefore, the decision variables $\mathbf{X}$ is defined as:

$$\mathbf{X} = [P^N_{SC,i},\ E^N_{SC,i},\ P^N_{SC,j},\ E^N_{SC,j},\ P^N_{DAB}]^T \tag{7}$$

1) Objective Functions

This paper adopts the minimization of the total life cycle cost (LCC) and the maximization of the RBE utilization rate as dual optimization objectives:

$$\begin{cases} \min F_{LCC}(\mathbf{X}) = C_{cap} + C_{om} + C_{grid} - C_{res} \\ \max F_{regen}(\mathbf{X}) = \dfrac{E_{total} - \sum\limits_{k\in\{i,j\}} \int_0^T P_{R,k}(t)\,dt}{E_{total}} \times 100\% \end{cases} \tag{8}$$

where C_{cap} is the initial investment cost; C_{om} is the operation and maintenance cost; C_{grid} is the grid electricity purchasing cost; C_{res} is the end-of-life asset salvage value; E_{total} is the total RBE generated by the system; and T is the total daily train operation duration. The specific calculations for each economic cost are as follows:

The initial investment cost C_{cap} encompasses the construction costs of the supercapacitors in each power supply section and the DAB:

$$C_{cap} = \sum_{k \in \{i,j\}} (c_p P_{SC,k}^N + c_e E_{SC,k}^N) + c_d P_{DAB}^N \tag{9}$$

where c_p and c_e are the unit power cost and unit capacity cost of the supercapacitor, respectively; c_d is the unit power cost of the dual active bridge converter.

The operation and maintenance cost C_{om} is converted using the capital discount method:

$$C_{om} = \sum_{y=1}^{Y} \left[\sum_{k \in \{i,j\}} c_{op} P_{SC,k}^N + c_{od} P_{DAB}^N \right] (1+r)^{-y} \tag{10}$$

where c_{op} and c_{od} are the annualized unit operation and maintenance costs for the supercapacitor and the DAB, respectively; r is the discount rate; and Y is the system life cycle.

The grid electricity purchasing cost C_{grid} consists of the energy charge and the basic capacity charge levied based on the maximum demand:

$$C_{grid} = \sum_{y=1}^{Y} (c_{eg} E_{grid} + 12 c_{dm} P_{max})(1+r)^{-y} \tag{11}$$

where c_{eg} is the energy price of the regional grid; E_{grid} is the total annual purchased electricity; c_{dm} is the monthly unit price for the basic demand charge; and P_{max} is the maximum demand of the substation.

The end-of-life asset salvage value C_{res} is calculated based on the salvage rate:

$$C_{res} = \sigma C_{cap} (1+r)^{-Y} \tag{12}$$

where σ is the end-of-life salvage rate of the equipment assets.

2) Constraints

Configuration Constraints:

$$\begin{cases} 0 \le P_{SC,k}^{N} \le P_{SC,k}^{max} \\ 0 \le E_{SC,k}^{N} \le E_{SC,k}^{max} \\ 0 \le P_{DAB}^{N} \le P_{DAB}^{max} \end{cases} \tag{13}$$

where $P_{SC,k}^{max}$ and P_{DAB}^{max} are the maximum planned rated powers for the supercapacitor and the DAB, respectively; $E_{SC,k}^{max}$ is the maximum planned rated capacity for the supercapacitor.

Operational Power Constraints:

$$\begin{cases} -P_{SC,k}^{N} \le P_{SC,k}(t) \le P_{SC,k}^{N} \\ -P_{DAB}^{N} \le P_{DAB}(t) \le P_{DAB}^{N} \end{cases} \tag{14}$$

State of Charge Constraints:

$$\begin{cases} SOC_{SC,k}^{\min} \le SOC_{SC,k}(t) \le SOC_{SC,k}^{\max} \\ SOC_{SC,k}(t+1) = \begin{cases} SOC_{SC,k}(t) - \dfrac{P_{SC,k}(t) \cdot \eta_{\text{ch}} \cdot \Delta t}{E_{SC,k}^{N}}, & P_{SC,k}(t) < 0 \\ SOC_{SC,k}(t) - \dfrac{P_{SC,k}(t) \cdot \Delta t}{E_{SC,k}^{N} \cdot \eta_{\text{dis}}}, & P_{SC,k}(t) > 0 \end{cases} \end{cases} \tag{15}$$

where $SOC_{SC,k}(t+1)$ and $SOC_{SC,k}(t)$ represent the state of charge of the energy storage medium at the next time step and the current time step, respectively; $SOC_{SC,k}^{\min}$ and $SOC_{SC,k}^{\max}$ are the minimum and maximum limits of the state of charge, respectively; η_{ch} and η_{dis} denote the charging and discharging efficiencies of the supercapacitor, and Δt is the energy storage scheduling time step.

3) Solution Algorithm

The system operation strategy and capacity configuration scheme are mutually coupled, jointly determining the overall economic and technical performance of the system. An excessively small capacity configuration cannot fully exploit the benefits of DAB-based cross-zone energy mutual support and peak shaving and valley filling via energy storage, whereas an excessively large configuration leads to prohibitively high investment costs. To address this, a bi-level optimization model considering operation scheduling and capacity configuration is established in this paper. Mathematically, this model belongs to the class of high-dimensional multi-objective mixed-integer nonlinear programming (MINLP) problems. For this complex optimization problem, the nondominated sorting genetic algorithm II with elitist strategy (NSGA-II) is employed to search for the global Pareto front, and the technique for order preference by similarity to ideal solution (TOPSIS) is introduced to make the final decision. The overall solution flowchart of the model is illustrated in Fig. 2.

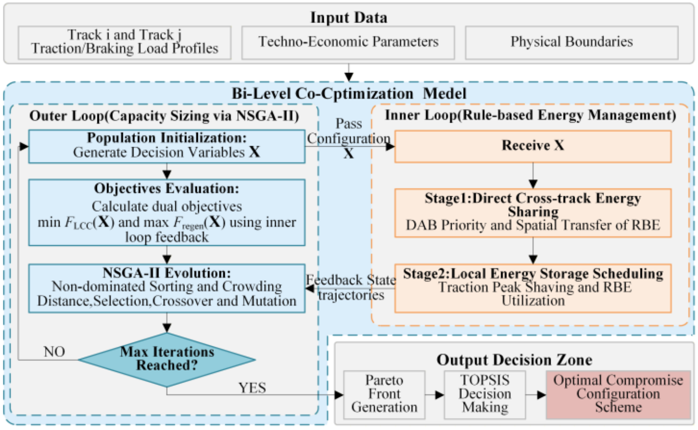

Figure 2: Overall solution flowchart of the model.

To guarantee the diversity and uniform distribution of the population, NSGA-II evaluates individuals based on non-dominated sorting and crowding distance. For an individual q residing in the same non-dominated rank, its crowding distance d_q is calculated as follows:

$$d_q = \sum_{m=1}^{M} \frac{f_m(q+1) - f_m(q-1)}{f_m^{max} - f_m^{min}} \tag{16}$$

where M is the total number of objective functions; $f_m(q+1)$ and $f_m(q-1)$ represent the objective values of the two adjacent points after sorting the individuals according to the m -th objective function; f_m^{max} and f_m^{min} are the maximum and minimum values of the m -th objective within that specific rank, respectively.

NSGA-II ultimately yields a set of non-dominated Pareto solutions. To filter out the optimal configuration scheme that successfully balances economics and energy efficiency, this paper incorporates the TOPSIS method for a posteriori decision-making. Since the life-cycle cost F_{LCC} is a cost-type metric and the RBE utilization rate F_{regen} is a benefit-type metric, the reciprocal of F_{LCC} is first taken to achieve directional alignment, followed by vector normalization to construct a standard decision matrix. Subsequently, the relative closeness C_q of each solution to the positive and negative ideal solutions is computed:

$$C_q = \frac{D_q^-}{D_q^+ + D_q^-} \tag{17}$$

where D_q^+ and D_q^- are the Euclidean distances from the q -th solution to the positive and negative ideal solutions, respectively. Ultimately, the solution exhibiting the maximum C_q is chosen as the recommended optimal compromise capacity configuration scheme for the system.

3 Results

3.1 Simulation Parameters and Case Setup

This paper conducts simulation verification based on the measured traction load data of a single train trip under two typical speed levels of 300 km/h and 430 km/h on the Shanghai high-speed maglev demonstration line. The key technical and economic parameters of the system are presented in Table 1.

Parameter [Unit]	Value
Project lifetime [Years]	20
Capital discount rate [%]	5
SC state of charge limits [%]	5 / 95
SC charge/discharge efficiency [%]	97
DAB power transmission efficiency [%]	95
Base demand charge [CNY/kW/month]	38.4
Grid energy price [CNY/kWh]	0.6790
SC power / capacity unit cost [CNY/kW / CNY/kWh]	1200 / 45000
DAB unit construction cost [CNY/kW]	460
SC / DAB annual O&M cost [CNY/kW/year]	21 / 10

Table 1: Key System Parameter Settings[11][13].

To conduct a comprehensive comparative performance analysis, three typical cases are set up in the simulation:

Case 1: Conventional TPSS, without ESS or DAB;
Case 2: TPSS integrated with ESS;
Case 3: Proposed architecture, TPSS integrating DAB and ESS..

3.2 Simulation Results and Analysis

The Pareto front of the LCC and RBE utilization rate obtained by solving Case 3 is shown in Fig. 3.

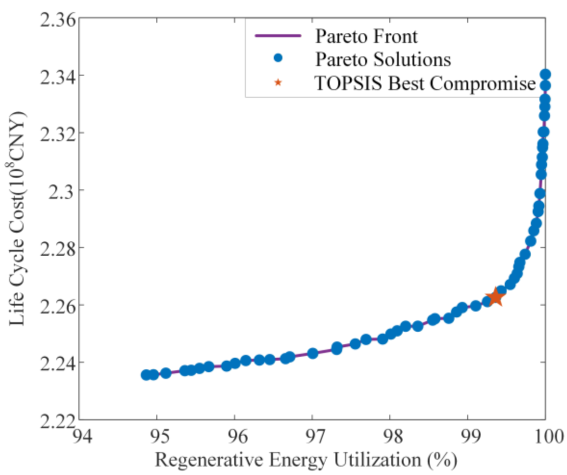

Figure 3: Pareto Front and TOPSIS Decision.

As shown in Fig. 3, there exists a significant trade-off relationship between the system economic cost and the RBE utilization rate. As the RBE utilization rate increases, the required energy storage capacity of the system rises markedly, leading to an upward trend in LCC. The star mark in the figure denotes the compromise optimal solution selected by the TOPSIS method, which effectively avoids the boundary effect caused by the extreme value of a single objective.

Parameter [Unit]	Case 1	Case 2	Case 3
Track i SC rated power / capacity [MW / MWh]	/	7.814 / 0.237	5.046 / 0.077
Track j SC rated power / capacity [MW / MWh]	/	7.845 / 0.237	7.775 / 0.238
DAB rated power [MW]	/	/	4.716
peak demand [MW]	6.77	5.80	5.41
Peak shaving rate [%]	/	14.38	20.11
RBE utilization rate [%]	0.00	99.87	99.36
Initial investment cost [10^4 CNY]	/	4328.93	3426.93
Operation and maintenance cost [10^4 CNY]	/	409.80	394.30
Electricity cost [10^4 CNY]	25063.55	19075.78	18869.60
Total life-cycle cost [10^4 CNY]	25063.55	23732.93	22626.24

Table 2: Optimization results of different cases.

Table 2 presents the optimization results of the three cases. As can be observed, in Case 2, each power supply zone requires an independently configured high-power and large-capacity ESS to smooth its own load fluctuations, resulting in an initial investment cost as high as 4328.93×10^4 CNY. In contrast, under the proposed architecture, the rated configurations of the ESS on both Track i and Track j are reduced, owing to the direct energy transfer path provided by the DAB converter. Notably, the power and capacity requirements of the ESS on Track i decrease by 35.4% and 67.5%, respectively, compared with Case 2, showing a particularly significant reduction. Although the introduction of the DAB adds certain equipment investment and operation and maintenance costs, the substantial reduction in ESS configuration requirements lowers the total initial investment cost to 3426.93×10^4 CNY, representing a 20.8% decrease relative to Case 2. This indicates that the cross-track power transfer mechanism effectively alleviates the transient buffering pressure on local energy storage and avoids costly redundant ESS deployment.

In terms of peak shaving performance, the proposed architecture, through the coordinated operation of the DAB and ESS, reduces the peak demand from 6.77 MW to 5.41 MW, achieving a peak shaving rate of 20.11%. This significantly mitigates the impact of high-power pulsating loads on the external utility grid and reduces the cumulative electricity cost over the entire life cycle to 18869.60×10^4 CNY, the lowest among the three cases. Meanwhile, the RBE utilization rate reaches 99.36%, which, though slightly lower than the 99.87% attained in Case 2, remains at an extremely high level, demonstrating that the proposed architecture achieves substantial economic improvement at a minimal cost in energy recovery. Overall, the proposed architecture strikes an effective balance among investment economy, peak shaving capability, and energy utilization efficiency, reducing the total life cycle cost to 22626.24×10⁴ CNY, the lowest value among the three cases, thereby validating the effectiveness and superiority of the proposed architecture and model.

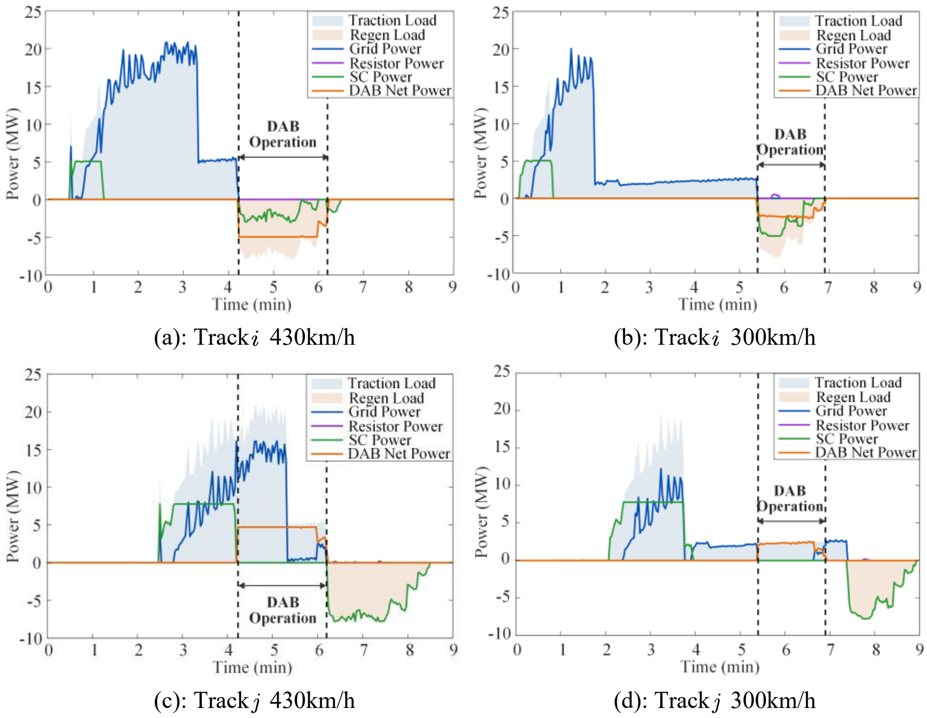

Figure 4: Dynamic Power Allocation with DAB.

Fig. 4 illustrates the power curves of each subsystem under typical operating conditions for the proposed architecture. As can be observed, when the two adjacent tracks exhibit complementary operating conditions—one under traction and the other under braking—the RBE can be immediately transferred across zones via the DAB converter to supply power to the traction train. Meanwhile, the supercapacitor not only effectively recovers the RBE of the braking train but also achieves peak shaving of the traction load.

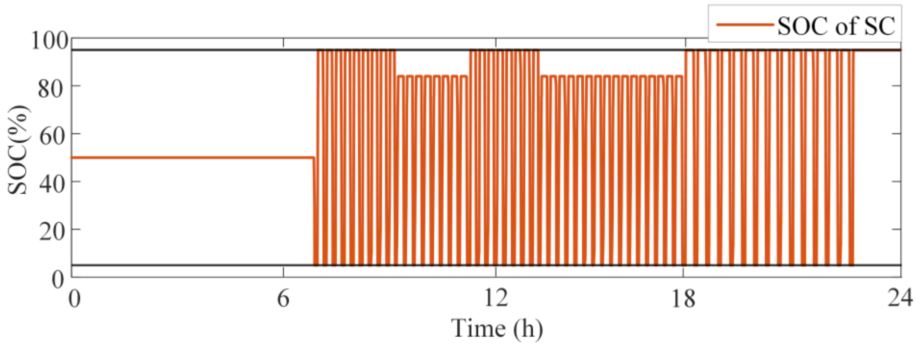

(a): Track i

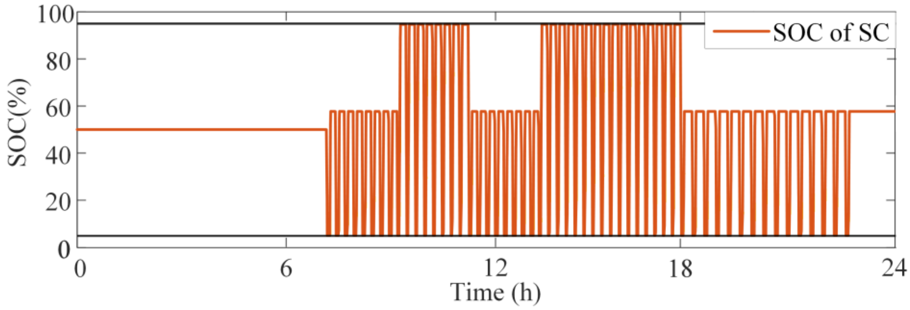

(b): Track j

Figure 5: SOC of SC.

Fig. 5 illustrates the SOC variation curve of the supercapacitor under the proposed architecture. As can be seen, the SOC of the supercapacitor is consistently maintained within the safe operating range of 5% to 95%, validating the effectiveness and safety of the energy management strategy.

4 Conclusions and Contributions

To address the challenge of low RBE utilization and the inability to share energy across zones in high-speed maglev transportation systems, this paper proposes a novel traction power supply architecture integrating a supercapacitor ESS and DAB converters, and establishes a bi-level optimization model considering both operation scheduling and capacity configuration. In the inner level, a rule-based energy management strategy is formulated to coordinate the power of each subsystem in real time; in the outer level, with the minimization of the total life cycle cost and the maximization of the RBE utilization rate as objectives, the NSGA-II algorithm combined with the TOPSIS method is adopted to solve for the optimal compromise configuration scheme. Validated with measured data from the Shanghai Maglev Demonstration Line, the results show that the proposed architecture significantly reduces the dependence on local energy storage capacity by constructing a direct cross-zone energy transfer path via the DAB converter, with the initial investment cost decreasing by 20.8% compared with the standalone ESS scheme. Under the optimal configuration, the system achieves an RBE utilization rate as high as 99.36% and a peak shaving rate of 20.11% at the substation, fully demonstrating its superior technical performance. The total life cycle cost is reduced to 22626.24×10^4 CNY, the lowest among the three comparative cases, verifying the economic advantages of the proposed architecture and optimization model. This study can provide theoretical reference and technical support for the design of energy-saving and economically efficient operation schemes for future high-speed maglev transportation systems.

Acknowledgements

This work was supported in part by the National Natura Science Foundation of China under Grant 52432012; and in part by the Open Foundation of the State Key Laboratory of High-speed Maglev Transportation Technology under Grant SKLM-SFCF-2023-010.

References

[1] G. Lin, W. Liu, J. Xu, Y. Sun, "Development opportunities and challenges of high-speed maglev transportation in China", Science and Technology Foresight, 2, 7-18, 2023.

[2] X. Gao, Z. Zhang, J. Zheng, "Energy consumption and efficiency analysis of high-speed maglev system", Technology Innovation and Application, 13, 30-36, 2023.

[3] S. Ding, "600 km/h High-Speed Maglev Transportation System", Shanghai Scientific and Technical Publishers, Shanghai, China, 2022.

[4] Y. Zhang, H. Hu, A. Geng, J. Chen, Y. Ge, K. Wang, "Capacity optimization configuration of hybrid energy storage system for electrified railway considering peak shaving and valley filling", Electric Power Automation Equipment, 43, 44-50, 2023.

[5] H. Hayashiya, S. Yokokawa, Y. Iino, H. Kondo, A. Okui, K. Ajiki, "Regenerative energy utilization in a.c. traction power supply system", in "Proceedings of the 2016 IEEE International Power Electronics and Motion Control Conference (PEMC)", IEEE, Piscataway, USA, 1125-1130, 2016.

[6] P. Wang, "Application analysis of regenerative braking energy feedback device in subway", Equipment Manufacturing Technology, 2, 169-172, 2023.

[7] J. Lin, S. Hu, Y. Li, J. Zhang, S. Wang, Y. Guo, M. Shahidehpour, "A Planning and Control-Integrated Design Approach for Railway Power Flow Controller With Hybrid Energy Storage System", IEEE Transactions on Intelligent Transportation Systems, 26, 1257-1272, 2025.

[8] Y. Ying, Z. Tian, M. Wu, Q. Liu, P. Tricoli, "Capacity Configuration Method of Flexible Smart Traction Power Supply System Based on Double-Layer Optimization", IEEE Transactions on Transportation Electrification, 9, 4571-4582, 2023.

[9] M.-H. Wang, S.-C. Tan, C.-K. Lee, S.Y.R. Hui, "A Configuration of Storage System for DC Microgrids", IEEE Transactions on Power Electronics, 33, 3722-3733, 2018.

[10] H. Dong, Z. Tian, J.W. Spencer, D. Fletcher, S. Hajiabady, "Bilevel Optimization of Sizing and Control Strategy of Hybrid Energy Storage System in Urban Rail Transit Considering Substation Operation Stability", IEEE Transactions on Transportation Electrification, 10, 10102-10114, 2024.

[11] M. Domínguez, A. Fernández-Cardador, A. Fernández-Rodríguez, A.P. Cucala, R.R. Pecharromán, "Review on the use of energy storage systems in railway applications", Renewable and Sustainable Energy Reviews, 207, 114904, 2025.
[12] Y. Zhang, "Research on capacity optimization configuration and economic evaluation method of hybrid energy storage system in electrified railway", Master's thesis, Southwest Jiaotong University, 2022.
[13] State Grid Shanghai Municipal Electric Power Company, "Shanghai Electric Power Company", [Online]. Available: https://www.sh.sgcc.cn. [Accessed: Apr. 28, 2026].